Polymer Chemistry

ROYAL SOCIETY OF CHEMISTRY

PAPER

View Article Online
View Journal | View Issue

Cite this: *Polym. Chem.*, 2025, **16**, 549

Self-healing and anti-oxidative mucus-inspired hydrogel†

Chunwen Tao,‡[a] Liyuan Peng,‡[a] Qiuyun Shao,[a] Kaihui Nan,*[a] Ravin Narain *[b] and Yangjun Chen *[a]

Received 19th September 2024,
Accepted 11th December 2024

DOI: 10.1039/d4py01042f

rsc.li/polymers

Natural mucus-inspired hydrogels have recently garnered significant attention in the fields of drug delivery and tissue engineering. Herein, we successfully prepared mucin-based hydrogels with self-repairing capability and antioxidant activity by employing rational material design principles. By harnessing Bigineli multicomponent reaction and free radical polymerization, antioxidant dihydropyrimidin(thio)one (DHPM) and phenylboronic acid (PBA) groups were facilely integrated onto a zwitterionic copolymer (denoted as PMPD). Furthermore, leveraging the abundant glycans present on mucin allowed for dynamic cross-linking through phenylboronic ester bonds with PBA moieties of PMPD to fabricate PM hydrogels. The dynamic nature of phenylboronic ester endowed PM hydrogels with excellent properties such as self-healing, injectable, and self-adaptable. Moreover, owing to the presence of DHPM antioxidant groups along with intrinsic antioxidant activity of mucin, PM hydrogels showed exceptional efficacy in scavenging free radicals. Additionally, PM hydrogel, which was prepared using natural mucin biopolymer and PMPD copolymer mimicking cell membrane structure, showed favorable cytocompatibility. Therefore, our current study represents a novel design strategy for multifunctional mucus-inspired hydrogels that hold promising potential for biomedical applications.

1. Introduction

Mucus, a biological dynamic hydrogel that serves as the primary defense against pathogens and external contaminants, is abundantly present at the biointerfaces covering various organs' underlying epithelial cells, including the eyes, mouth, nose, gastrointestinal tract, respiratory system, and genital tracts.[1,2] For instance, mucus safeguards the ocular surface by providing lubrication to the underlying tissue and dissipating energy generated from eye blinking to prevent desiccation.[3–5] However, both physiological conditions and pathological circumstances can alter mucus composition and compromise its protective barrier function. Taking dry eye disease (DED) as an example of such alteration, tear film hyperosmolarity triggers an inflammatory response leading to reduced expression of glycocalyx mucins along with apoptotic death of surface epithelial cells and loss of goblet cells responsible for secreting gel-forming mucins.[4] Consequently, artificial tears that emulate the lubricating properties of natural mucins are extensively employed in DED treatment.[6] However, their therapeutic efficacy remains limited primarily due to the absence of functional attributes such as anti-inflammatory and antioxidant properties, underscoring the significance of the development of novel mucus-inspired biomaterials for treating mucosal diseases.

Mucus primarily consists of mucins, a class of glycoproteins that exhibit a bottle-brush structure characterized by a protein backbone and radially arranged oligosaccharide side chains.[7] Notably, these side chains can account for approximately 80% of the overall mass of mucin. Exploiting the unique chemical structures and biological properties of mucin, hydrogels based on this biomolecule have emerged as promising substitutes for native mucus in the treatment of diseases associated with mucosal dryness,[8] providing epithelial protection and lubrication. For instance, Lieleg *et al.* demonstrated exceptional lubricity and antifouling behavior by covalently coating contact lenses with mucin biomacromolecules to prevent dry eye symptoms.[9,10] Furthermore, they developed methacryloyl-functionalized purified mucin hydrogels for

[a]*National Engineering Research Center of Ophthalmology and Optometry, Institute of Biomedical Engineering, School of Ophthalmology & Optometry, Eye Hospital, Wenzhou Medical University, Wenzhou, Zhejiang 325027, China.*
E-mail: nankh@wmu.edu.cn, chenyj@wmu.edu.cn
[b]*Department of Chemical and Materials Engineering, College of Natural and Applied Sciences, University of Alberta, Edmonton, Alberta T6G 2G6, Canada.*
E-mail: narain@ualberta.ca

†Electronic supplementary information (ESI) available: The ^{1}H NMR spectrum of PBA-DHPM monomer, aqueous GPC curve of PMPD copolymer, frequency sweeps of P1M1 and P2M1 hydrogels, self-healing behavior, ABTS$^+$ radical scavenging ability of PMPD copolymer and mucin, cytotoxicity of PMPD copolymer, and culture medium containing 10% DMSO (positive control). See DOI: https://doi.org/10.1039/d4py01042f

‡These two authors contributed equally to this work.

various biomedical applications including drug delivery and 3D bioprinting.[11–13]

As is widely recognized, mucin forms a mucus hydrogel through dynamic disulfide cross-linking, prompting researchers to explore nature-inspired strategies for developing mucus-mimicking hydrogels.[14] For example, hydrogels can be prepared by dynamically cross-linking mucin with thiol-functionalized polyethylene glycol (PEG) derivatives.[15] Interestingly, the abundant presence of glycans on mucin offers the potential for forming dynamic hydrogels *via* phenylboronic acid (PBA)-diol complexation.[16–18] PBAs have been extensively investigated for their ability to form phenylboronic ester bonds with *cis*-diol-containing molecules such as sugars,[19–21] polyphenols,[22–25] and synthetic polymers like poly(vinyl alcohol) (PVA).[26–28] Furthermore, PBA-modified nanosystems that can specifically bind to sialic acid residues in mucin have been widely employed in mucoadhesive strategies to achieve prolonged mucosal retention and enhanced drug delivery.[29–35] Recently, Sumerlin *et al.* developed a novel copolymer containing PBA moieties that successfully formed a hydrogel with natural mucin through phenylboronic ester cross-linking,[36] demonstrating promising potential for the advancement of mucus-inspired hydrogels using natural mucin and synthetic PBA-modified hydrophilic polymers. In terms of hydrophilic polymers, zwitterionic polymers exhibit superior performance compared to other options such as PEG and poly(*N*,*N*-dimethylacrylamide).[37–43] Notably, 2-methacryloyloxyethyl phosphorylcholine (MPC)-based zwitterionic polymers with cell membrane-mimicking structures have been extensively studied due to their excellent antifouling and lubricating properties akin to mucin.[44–50] Therefore, the cross-linking between PBA-modified MPC-based copolymers and mucin represents a more biomimetic strategy for developing mucus-inspired dynamic hydrogels.

It is worth noting that inflammatory and oxidative stress often exist in mucosal diseases.[51–53] For example, oxidative stress induced by elevated levels of reactive oxygen species (ROS) has been demonstrated to promote the vicious cycle of DED as an upstream pathway of inflammation.[53–55] Antioxidants such as cerium-based nanozymes have gained widespread application in treating inflammatory mucosal damage disorders like DED, ulcerative colitis, acute gastroenteritis, among others.[56–59] Therefore, the development of mucin-based hydrogels with ROS scavenging capability holds tremendous potential for addressing these conditions.

Taking all above into account, we aimed to develop multifunctional mucin-based hydrogels through dynamic cross-linking of phenylboronic acid ester (Fig. 1). Firstly, a zwitterionic copolymer PMPD containing antioxidant DHPM groups and phenylboronic acid residues was synthesized by harnessing Bigineli multicomponent reaction and free radical polymerization. Then, PMPD was mixed with mucin solution to form PM hydrogels *via* the formation of phenylboronic ester bonds. The self-healing and injectable properties of the resulting PM hydrogels were investigated through rheological analysis and macroscopic observation. Moreover, the antioxidant activity of the PMPD copolymer, mucin, and PM hydrogel was carefully evaluated. The cytocompatibility of the PM hydrogel was further assessed using both CCK-8 assay and Live/Dead staining method. Our study may provide new insights into developing novel multifunctional mucus-inspired hydrogels for potential biomedical applications in treating mucosal diseases.

2. Experimental section

2.1. Materials

MPC monomer was obtained from Tokyo Chemical Industry Co., Ltd (TCI Shanghai, China). 2-(Acetoacetoxy) ethyl methacrylate (AEMA), 4-formylphenylboronic acid (FPBA), thiourea,

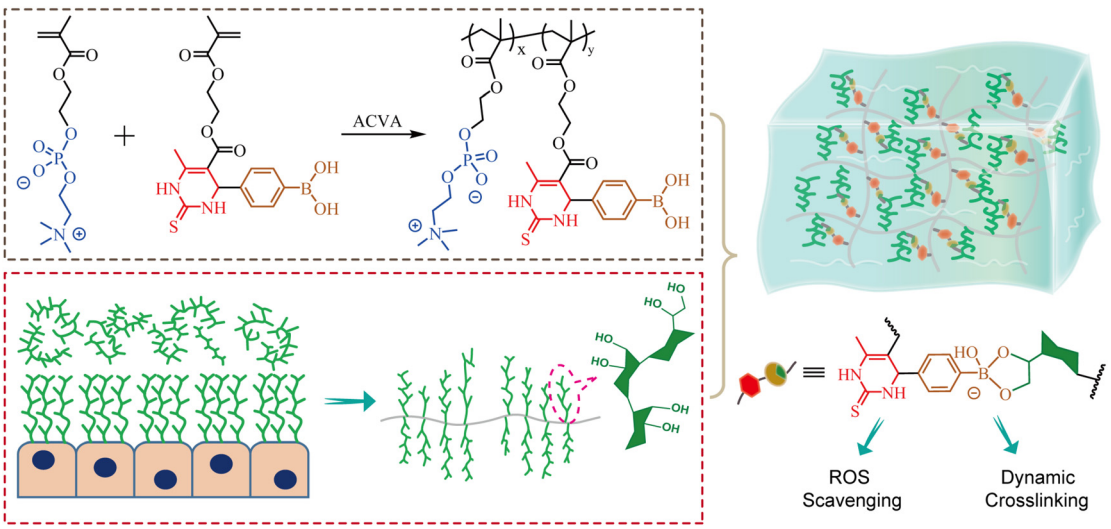

Fig. 1 Schematic illustration of the molecular structure of functional zwitterionic PMPD copolymer and the preparation of mucus-inspired hydrogel through dynamic phenylboronic ester cross-linking.

magnesium chloride ($MgCl_2$), acetic acid, methylene blue (MB), and rhodamine B (RhB) were purchased from Macklin Biochemical Co., Ltd (Shanghai, China). 4,4′-Azobis (4-cyanovaleric acid) (ACVA) and hydrogen peroxide (H_2O_2, 30%) were bought from Sigma Aldrich (Saint Louis, MO, USA). *N*,*N*-dimethylformamide (DMF), methanol, and other solvents were obtained from J&K Scientific (Beijing, China). Porcine stomach mucin and dialysis membrane bags (MWCO: 6000–8000 Da) were obtained from Yuanye Bio-Technology Co., Ltd (Shanghai, China). 2,2′-Azino-bis (3-ethylbenzothiazoline-6-sulfonic acid) ammonium salt (ABTS) and ROS assay kit (2′,7′-dichlorodihydrofluorescein diacetate, DCFH-DA) were obtained from Beyotime Biotech. Inc. (Shanghai, China). Live/Dead assay kit (calcein-AM/ethidium homodimer-1), Dulbecco's Modified Eagle's medium: Nutrient Mixture F-12 (DMEM/F12), 0.25% trypsin with 0.02% ethylene diamine tetraacetic acid (EDTA), and fetal bovine serum (FBS) were purchased from Thermo Fisher Scientific (USA). Cell counting kit-8 (CCK-8) was obtained from Dojindo Laboratories (Japan). The functional monomer (PBA-DHPM) with PBA and DHPM moieties was synthesized *via* the Biginelli reaction according to previous reports.[60] Other reagents were of analytical grade and used as received unless specifically noted.

2.2 Synthesis of zwitterionic copolymer (PMPD)

The zwitterionic copolymer was synthesized by free radical polymerization using MPC and PBA-DHPM as monomers and ACVA as the initiator. Briefly, MPC (1.50 g, 5.1 mmol), PBA-DHPM (363.6 mg, 0.9 mmol), and ACVA (8.4 mg, 0.03 mmol) were dissolved in a mixture of DMF and methanol. The mixed solution was thoroughly purged with nitrogen gas for 30 min. After that, the vessel was sealed and placed in a preheated oil bath at 70 °C, and the reaction was allowed to be kept overnight. The polymerization was stopped by rapid cooling in an ice bath and exposure to the air. The zwitterionic copolymer was purified by precipitation twice into acetone to remove unreacted monomers and further dialysis against Milli-Q water for 24 h. PMPD copolymer was finally obtained after lyophilization.

2.3 Preparation of PM hydrogels

PM hydrogels were prepared based on dynamic phenylboronic ester cross-linking between commercially available porcine stomach mucin and PMPD copolymer. Three hydrogels were prepared by mixing PMPD (10 w/v%) and mucin (4 w/v%) solutions with different volume ratios (1 : 2, 1 : 1, and 2 : 1). The resulting hydrogels were named as P1M2, P1M1, and P2M1, respectively. The formation of hydrogels was macroscopically observed *via* a vial-titling method.

2.4 Characterization

^{1}H NMR spectra of PBA-DHPM monomer and PMPD copolymer were recorded on a Bruker Avance spectrometer at 400 MHz using DMSO-d_6 or a mixture of CD_3OD and DMSO-d_6 as solvent. The number (M_n) and weight (M_w) average molecular weight and polydispersity index (PDI = M_w/M_n) of the zwitterionic copolymer were determined by an aqueous gel permeation chromatography (GPC) system (170 waters1525 & Agilent PL-GPC220, USA). The GPC was calibrated by monodisperse polyethylene oxide (PEO) standards. The porous morphology of hydrogels was observed by a scanning electron microscopy (SEM) (Zeiss Sigma 300, Carl Zeiss AG, Germany). The hydrogels were freeze-dried and sputter-coated with gold to provide a conductive environment prior to SEM observation. The mechanical and self-healing properties of hydrogels were investigated through a rheometer (DHR-2, TA Instruments, USA) with a 25 mm diameter aluminum parallel plate geometry at 25 °C. The storage modulus (G') and loss modulus (G'') values *versus* frequency in the range of 0.1 rad s^{-1} to 100 rad s^{-1} were recorded at a constant strain of 1% to study the mechanical property. The hydrogel was also tested by oscillatory strain amplitude sweep from 0.1% to 1000% with the frequency kept at 1 Hz. The critical strain required for gel failure was determined at the crossover point of G' and G''. Then, a step-strain test was performed to study the self-recovery ability of hydrogels by repeating large strain (500%, 30 s) for network disruption and small strain (1%, 60 s) for mechanical recovery.

2.5 Self-healing, self-adaptable, and injectable properties

The self-healing, self-adaptable, and injectable properties of PM hydrogels were further investigated *via* macroscopic observation. To study the self-healing ability, two disk-shaped hydrogels were stained with rhodamine B and methylene blue, respectively. These two hydrogels were exposed without external stimulation. Once the contact area at the edge disappears, the joined hydrogel was lifted up by using two tweezers from both ends, and then stretched to assess any potential rupture of the contact surface. To evaluate the injectability, a mixture of 3 mm and 2 mm steel beads was introduced into a bottle, followed by injecting PM hydrogel onto the surface of the steel beads using a syringe. Photographs were taken to record the process of hydrogel permeation and pore filling within the steel beads. For assessing injectability, an appropriate volume of rhodamine B-stained hydrogel was loaded into a syringe and injected into a bottle containing PBS using a 26 G needle. Furthermore, the hydrogel was further served as 'ink' for inscribing 'MUCIN' *via* the syringe needle.

2.6 Antioxidant activity *via* ABTS assay

The $ABTS^+$ radical scavenging assay was employed to quantify the overall antioxidant capacity of PMPD copolymer, mucin, and PM hydrogels. Upon reaction with an oxidizing agent, ABTS forms a stable blue-green $ABTS^+$ radical with a maximum absorption peak at 734 nm. The addition of antioxidants leads to the disappearance of the blue-green color in reaction with $ABTS^{\bullet+}$. To prepare the working solution of $ABTS^{\bullet+}$, equal volumes of $ABTS^+$ and oxidizing agent solutions were combined in a 1 : 1 ratio and incubated at room temperature in darkness for 12 hours. Subsequently, the resulting mixture was diluted with PBS until an absorbance value of 0.7 ± 0.05 at 734 nm was achieved.

The $ABTS^+$ radical scavenging abilities of PMPD polymer and mucin were assessed initially. PMPD or mucin was weighed and dissolved in PBS with gradient dilutions to achieve concentrations of 1, 3, 5, and 10 mg mL^{-1}. The control group was prepared using a PBS solution. For qualitative observation, sample bottles were prepared by adding 75 μL of either PBS or the material solution followed by the addition of 1.5 mL of $ABTS^{\bullet+}$ working solution. Color changes were documented every 10 min through photography. For quantitative measurement, a blank group consisting of 210 μL of PBS was prepared in a 96-well plate. The control group (control) and experimental groups each received an additional dose of either 10 μL PBS or the material solution followed by the addition of 200 μL $ABTS^{\bullet+}$ working solution. Absorbance changes at 734 nm were immediately measured using a microplate reader to calculate the clearance rate for $ABTS^+$ free radicals.

The free radical scavenging capability of PM hydrogels was further measured by ABTS assay. Briefly, 0.5 mL of P2M1, P1M1, and P1M2 hydrogel were loaded in glass vials separately. Subsequently, 2.5 mL of $ABTS^{\bullet+}$ working solution was added to each vial and photographs were captured to record color changes. After 30 min and 60 min, 100 μL of the supernatant was promptly collected and transferred into a 96-well plate. The absorbance at 734 nm was measured using a microplate reader.

2.7 Cell culture

The human corneal epithelial cells (HCECs) and human conjunctival epithelial cells (HCJECs) were obtained from Procell Life Science and Technology Co., Ltd (Wuhan, China). The cells were cultured in DMEM/F-12 medium supplemented with 10% FBS and 1% penicillin–streptomycin, and incubated at 37 °C with 5% CO_2 in a thermostat incubator.

2.8 Cell cytotoxicity

The HCEC or HCJEC cells were seeded in 96-well plates at a density of 8000 cells per well. After 24 h, the culture medium was replaced by fresh medium containing PMPD copolymer at different concentrations of 0.1, 0.2, 0.5, 1, 2, 5, and 10 mg mL^{-1}. Continuous cultivation was carried out for an additional 24 h or 48 h. The culture medium was subsequently removed, and 100 μL of CCK-8 working solution was added to each well. The optical density (OD) values at 450 nm were measured on a microplate reader.

The cytotoxicity of gel extracts was evaluated similarly using CCK-8 assay by replacing PMPD solution with gel extracts, which were obtained by co-culturing PM hydrogel with culture medium at different volume ratios (1 : 10, 1 : 20, 1 : 40) for 24 h. Live/Dead staining assay was further used to evaluate the cytocompatibility of gel extracts. Cells were incubated with gel extracts for 24 or 48 h. After washing with PBS, a mixture of Calcein-AM (Green fluorescence indicates living cells) and ethidium homodimer-1 (Red fluorescence indicates dead cells) was introduced into wells. Fluorescence images were obtained by using an EVOS microscope.

2.9 Intracellular ROS scavenging assessment

The DCFH-DA probe was utilized to measure ROS levels within cells. HCECs were seeded into a 24-well plate at a density of 5 × 10^4 cells per well and allowed to adhere and grow for 24 h. Subsequently, fresh medium containing 400 μM H_2O_2 was added to induce intracellular ROS stimulation. In the experimental group, a Transwell insert containing 100 μL PM hydrogel was also included. After co-incubation for 1 h, the Transwell insert was removed, and the cells were further cultured for an additional 3 h. The cells treated with normal culture medium and culture medium containing 400 μM H_2O_2 for 4 h were set as the negative control and positive control, respectively. Following PBS washing, the cells were incubated with DCFH-DA (10 μM) in serum-free DMEM/F-12 for 25 min at 37 °C in darkness. Fluorescence images were then captured using a DMi8 fluorescence microscope (Leica, Germany).

3. Results and discussion

3.1 Synthesis and characterization of PMPD copolymer

The hydrogel precursor, *i.e.* zwitterionic copolymer PMPD, was prepared by free radical polymerization of MPC and PBA-DHPM monomers. MPC-based zwitterionic polymers have gained significant attention as an FDA approved highly hydrophilic biomaterial and have found extensive applications in various biomedical fields, including antifouling surface modification and long-term blood circulation for *in vivo* drug delivery. Recently, Tao *et al.* reported the utilization of the dual functionalized monomer, PBA-DHPM, to fabricate functional polymers capable of constructing antioxidant hydrogels for 3D cell culture.[60] In the present work, PBA-DHPM was co-polymerized with MPC at a mole ratio of 15%, thus endowing the PMPD copolymer with both hydrophilicity and multifunctionality. The chemical composition of PMPD was studied by ^1H NMR (Fig. 2). The chemical assignments of various peaks were

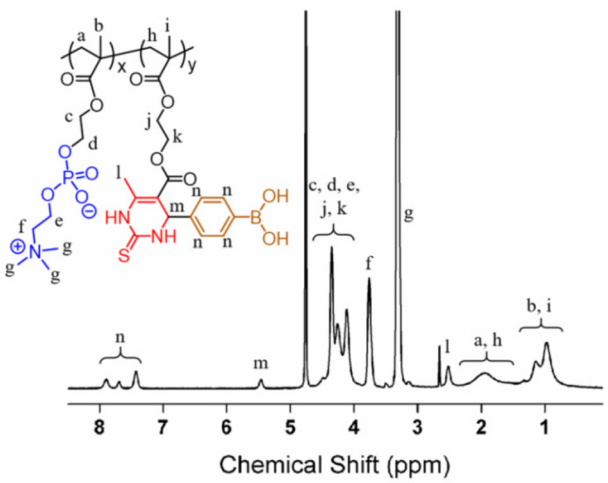

Fig. 2 The chemical structure and ^1H NMR spectrum of zwitterionic PMPD copolymer.

clearly discernible, including characteristic peaks of MPC such as –N(C**H**$_3$)$_3$ (δ 3.07–3.55 ppm, marked as "g") and –C**H**$_2$–N(CH$_3$)$_3$ (δ 3.76 ppm, marked as "f"), as well as benzene ring characteristic peaks of PBA-DHPM (δ 7.42, 7.69, 7.89 ppm, marked as "n"). By comparing the integral of H_n to that of H_f, the final molar ratio of PBA-DHPM in the copolymer was calculated to be ~13.9%, which is in good agreement with the feed ratio, suggesting the successful synthesis of PMPD copolymer. Furthermore, the molecular weight of PMPD was measured to be 2.56×10^4 Da *via* aqueous GPC (Fig. S2†). The polydispersity index (PDI) was determined to be ~2.49 due to the uncontrollable nature of free radical polymerization.

3.2 Preparation and characterization of hydrogels

The hydrogels were prepared by pipetting a mixture of PMPD (10 w/v%) and mucin (4 w/v%) solutions with varying volume ratios (1 : 2, 1 : 1, 2 : 1). The resulting hydrogels were named as P1M2, P1M1, and P2M1, respectively. As shown in Fig. 3A, upon mixing PMPD and mucin solutions in their liquid state, the fluidity rapidly changed within a span of 30 s, ultimately leading to prompt gelation as confirmed by employing the bottle-tilting method. The rapid gelation can be attributed to the efficient formation of dynamic phenylboronic ester bonds between the PBA moieties of PMPD and sialic acid residues of mucin.

The microstructure of the freeze-dried PM hydrogels was then observed using SEM, as depicted in Fig. 3B. Three types of hydrogels, prepared by varying the volume ratios of PMPD and mucin solutions, all exhibited a three-dimensional (3D) porous network structure. The presence of porous architecture is believed to facilitate efficient nutrient and oxygen transfer and exchange, thereby rendering these hydrogels highly promising for biomedical applications such as drug delivery, 3D cell culture, and tissue engineering, including corneal regeneration.

Rheological measurements were applied to investigate the mechanical properties of PM hydrogels. Initially, frequency sweep was conducted to compare the mechanical strength of P1M2, P1M1, and P2M1 hydrogels. All three hydrogels exhibited frequency-dependent viscoelastic behavior, with a crossover point (where $G' = G''$) observed at 1.29 (Fig. 4A), 1.15 (Fig. S3†), and 1.00 (Fig. S4†) rad s^{-1} respectively. This observation demonstrated the characteristic behavior of dynamic hydrogel networks relying on reversible phenylboronic ester cross-linking. The storage modulus at a fixed frequency of 10 rad s^{-1} was measured as 1988.7 Pa, 2882.7 Pa, and 1934.1 Pa for P1M2, P1M1, and P2M1 hydrogels respectively. The variation in G' values can be attributed to differences in solid content and variations in the PBA : diol ratio among these hydrogels. Subsequently, P1M2 hydrogel was chosen for further rheological examinations. An oscillation strain sweep ranging from 0.1% to 1000% was performed on this sample at a fixed frequency of 1 Hz. As the strain increased, the modulus initially underwent a plateau and then exhibited an inversion with G''surpassing G', indicating gel failure under such strain conditions (Fig. 4B). The critical strain value required to disrupt the hydrogel network (crossover strain, where $G' = G''$) was determined as 209.4%. To evaluate the self-healing capability of P1M2 hydrogel, a step-strain sweep experiment alternating between low (l%) and high (500%) strains was carried out. As shown in Fig. 4C, when subjected to a large strain of 500%, the hydrogel network was destroyed, resulting in a

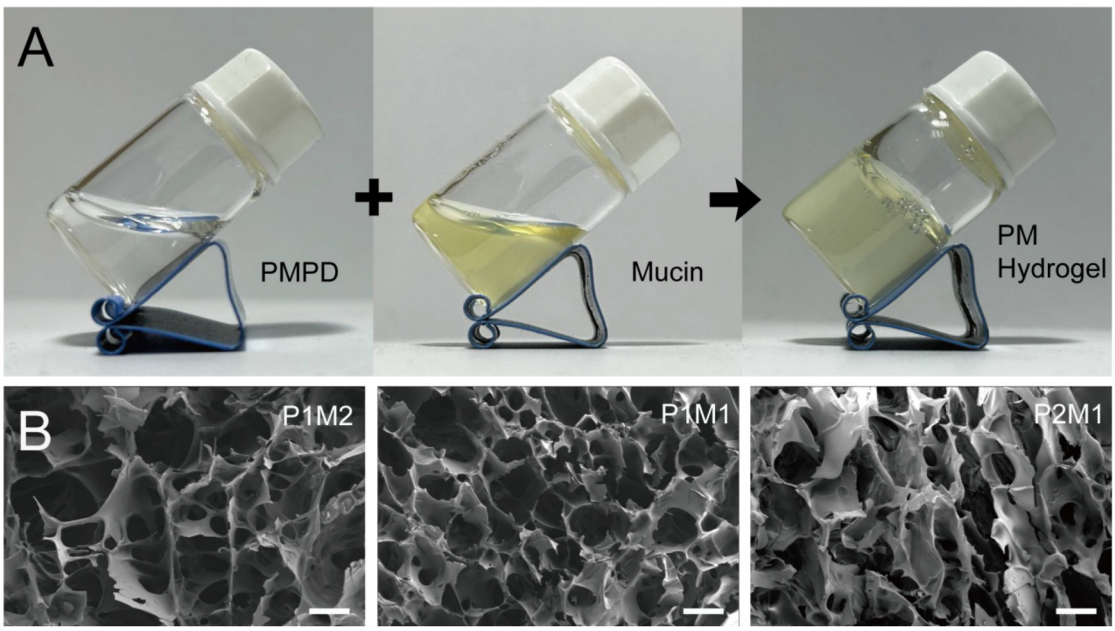

Fig. 3 (A) Formation of hydrogel *via* mixing the solutions of PMPD and mucin. (B) SEM images of P1M2, P1M1, and P2M1 hydrogels. Scale bar = 100 μm.

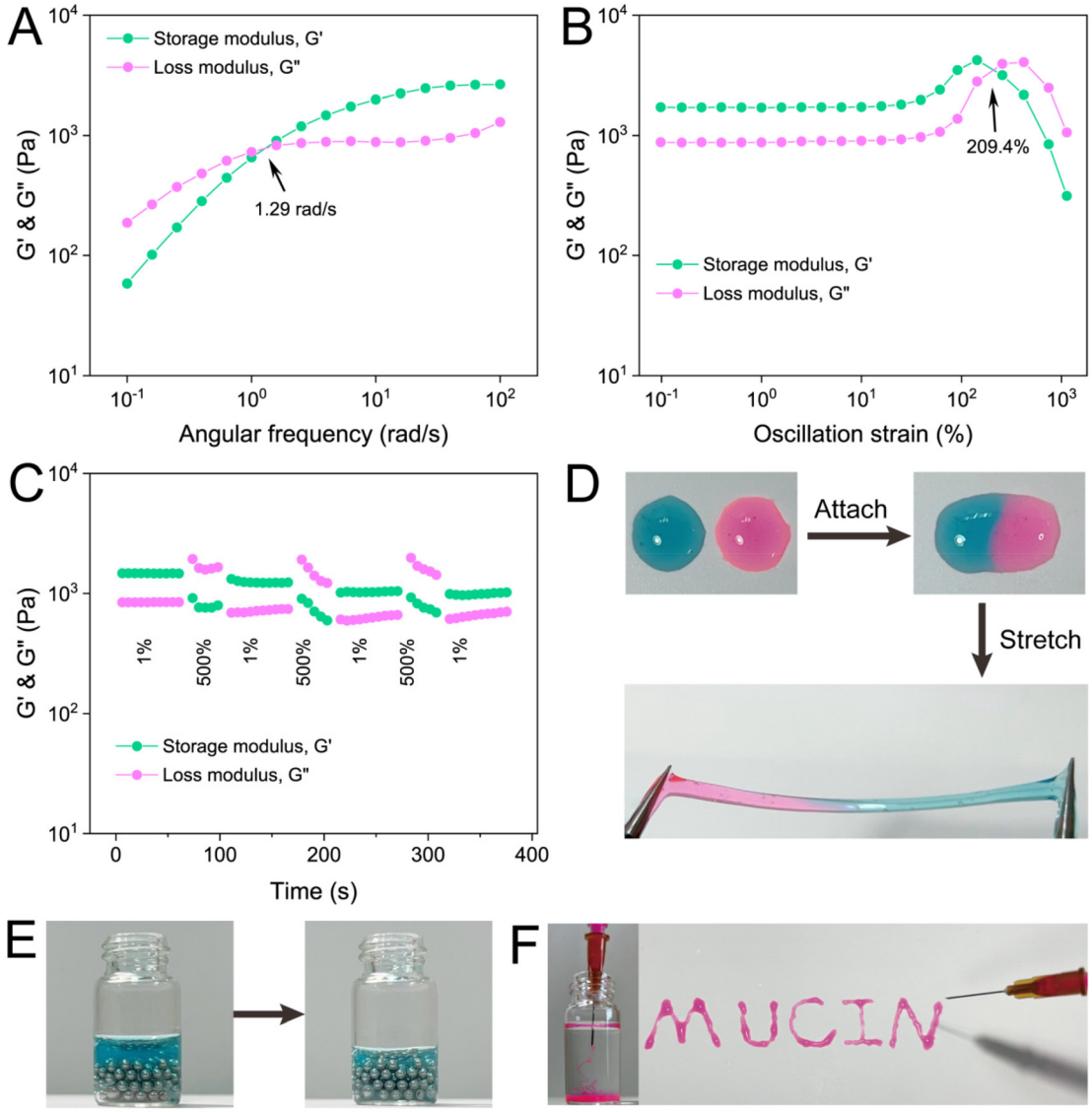

Fig. 4 (A) Frequency sweep of P1M2 hydrogel in the range of 0.1 to 100 rad s^{-1} at a fixed strain of 1%. (B) Strain sweep of P1M2 hydrogel in the range of 0.1% to 1000% at a fixed frequency of 1 Hz. (C) The change of G' and G'' values of P1M2 hydrogel with alternating strains of 1% and 500%. (D) Macroscopic observation of the self-healing property. (E) Self-adaptable property of the hydrogel. (F) The injectable property of P2M1 hydrogel *via* (i) injecting the hydrogel into PBS and (ii) writing a word of "MUCIN" through a syringe needle.

liquid state with a higher G'' over G'. Intriguingly, almost complete recovery of the G' value could be immediately achieved by applying a small strain of 1% to the hydrogel, demonstrating rapid self-healing efficiency. Furthermore, this "destruction-repair" cycle could be readily repeated for at least three iterations, highlighting the remarkable reversibility of phenylboronic ester bonds between PMPD and natural mucin biopolymer.

3.3 Self-healing, injectable, and self-adaptable properties

The excellent reversibility of phenylboronic ester has been widely reported to endow hydrogels with good self-healing property.[17] Upon placing two pieces of PM hydrogel, stained separately with rhodamine B and methylene blue dyes, in close proximity, the contact surface undergoes rapid disappearance within a span of 30 s (Fig. 4D), indicating complete fusion of the hydrogels into a unified entity. Notably, no signs of tearing were observed at the connection point when manipulated with tweezers. Furthermore, the hydrogel exhibits exceptional stretchability as it could be elongated up to four times its original length while maintaining structural integrity.

The phenylboronic ester in PM hydrogels demonstrates high dynamic reversibility, constantly undergoing a cycle of "breakage-reconstruction", which showcases its exceptional adaptability. As depicted in Fig. 4E, when placed on an uneven surface composed of steel beads, the hydrogel swiftly moved downward under gravity within 3 min, effectively filling the gaps between them. This observation highlighted the excellent self-adaptability of PM hydrogels.

Hydrogels based on dynamic crosslinking often exhibit injectability. As depicted in Fig. 4F, the hydrogel could be easily injected into a PBS solution using a 1 mL syringe needle (26G). After injection, the gel remained structurally stable. Additionally, the hydrogel could serve as "ink" for writing words (MUCIN) through a syringe needle (Fig. 4F). These findings underscored the excellent injectability of PM hydrogels.

3.4 *In vitro* antioxidant activity and intracellular ROS scavenging evaluation

The total antioxidant capacity of PMPD, mucin, and the resulting PM hydrogels was assessed using the ABTS method. As depicted in Fig. S5,† upon mixing $ABTS^{\bullet+}$ with different concentrations of PMPD copolymer solutions, the initial bluish-green color of $ABTS^{\bullet+}$ gradually diminished over time. Remarkably, the mixed solution with 10 mg mL^{-1} PMPD became colorless after 60 min, indicating near-complete elimination of $ABTS^{\bullet+}$. The scavenging activity was calculated by measuring the OD values at 734 nm and presented as a dual dependence on concentration and time (Fig. S6†), in accordance with visual observations. The remarkable free radical scavenging capability of PMPD should be primarily attributed to its DHPM moieties, as previously reported by Tao *et al.*[60] Interestingly, we found that mucin also exhibited notable free radical scavenging capability, exhibiting similarly time- and concentration-dependent clearance of $ABTS^{+}$ radicals (Fig. S7†). This phenomenon is consistent with previous findings that have also demonstrated the antioxidant capacity of mucin,[61,62] which can be attributed to its abundant cysteine[63] and sialic acid[64] residues. At the highest concentration tested (10 mg mL^{-1}), a significant reduction in color intensity occurred with a scavenging rate reaching up to 69.5% (Fig. S8†). These findings highlight the excellent anti-oxidative properties possessed by both PMPD and mucin.

Subsequently, the ABTS method was employed to further investigate the antioxidant activity of PM hydrogels. As shown in Fig. 5A, upon mixing P2M1, P1M1, and P1M2 hydrogels with ABTS working solution at a volume ratio of 1 : 5 separately, the color intensity of $ABTS^{\bullet+}$ solution rapidly diminished within 60 min, indicating that all three hydrogels exhibited remarkable capacity for rapid removal of $ABTS^{+}$ radicals within a short duration. Additionally, it can be clearly observed that the color diminishing speed at 30 min followed a trend of P2M1 > P1M1 > P1M2. The free radical scavenging rates at

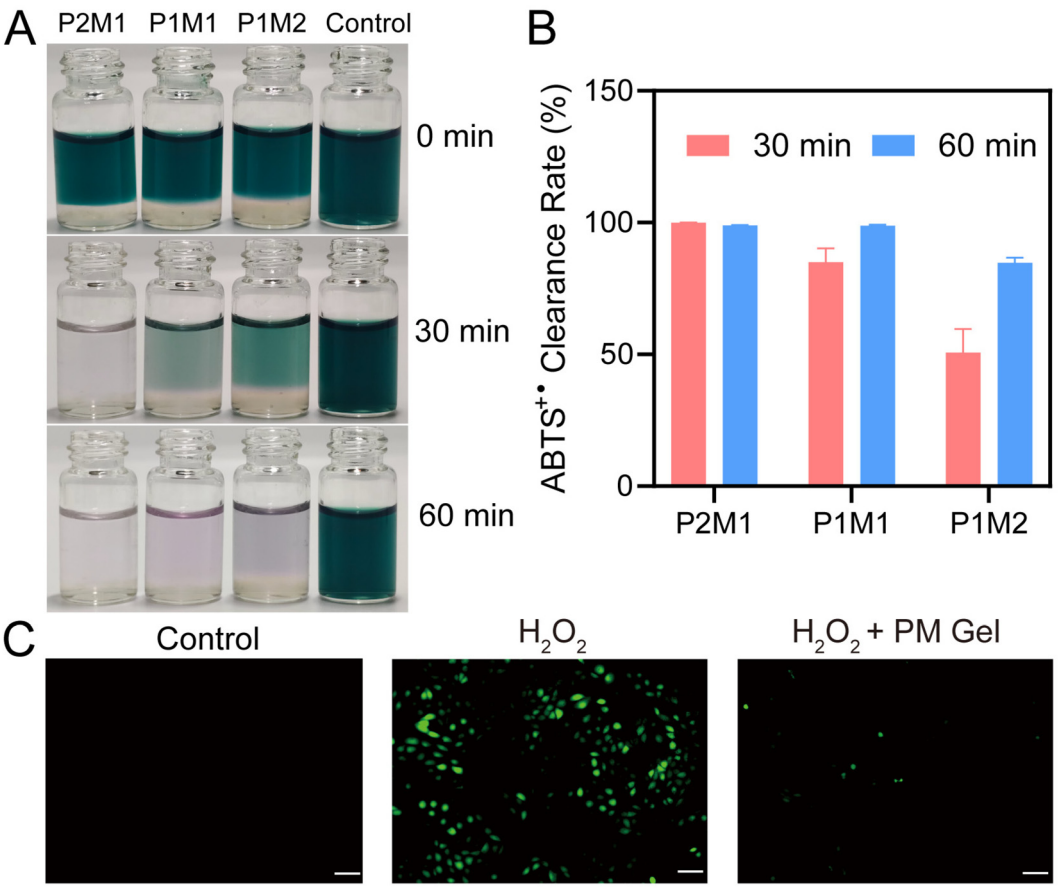

Fig. 5 (A) Photographs of $ABTS^{\bullet+}$ solutions co-incubated with P2M1, P1M1, and P1M2 hydrogels for (i) 0 min, (ii) 30 min, and (iii) 60 min. (B) The $ABTS^{\bullet+}$ scavenging efficiency of PM hydrogels after co-incubation for 30 and 60 min. (C) Intracellular ROS-scavenging capability of PM hydrogel as monitored by DCFH-DA probe. Scale bar = 100 μm.

30 min were measured as 99.9%, 84.9%, and 50.7% for P2M1, P1M1, and P1M2 respectively (Fig. 5B), aligning well with the macroscopical observation result. The variation in $ABTS^{\bullet+}$ clearance rate among these hydrogels can be attributed to their different proportions of mucin and PMPD components. Notably, the P2M1 hydrogel with the highest content of PMPD exhibited superior free radical scavenging efficiency.

The intracellular oxidative stress model was further established by stimulating HCECs with H_2O_2 to evaluate the ROS-scavenging capacity of PM hydrogels. As shown in Fig. 5C, a significant increase in green DCF fluorescence was observed following treatment with 400 μM H_2O_2. In contrast, co-incubation of H_2O_2-stimulatd HCECs with PM hydrogel resulted in a substantially lower level of green fluorescence, comparable to the normal standard (control group). These findings further validate the outstanding antioxidant property of PM hydrogels.

Oxidative stress is widely recognized as being implicated in the pathogenesis of various diseases. Consequently, PM hydrogels possessing exceptional anti-oxidative property hold promising potential for treating diseases by functioning as ROS scavengers. For example, elevated ROS level and decreased amount of mucin are usually found in the ocular surface of DED.[65] Hence, PM hydrogels can potentially serve as an ROS scavenger as well as a mucin additive to regulate the pathological microenvironment, thereby promoting the treatment of DED.

3.5 Cytocompatibility of PM hydrogels

For potential biomedical applications, excellent biocompatibility is one of the most important prerequisites. As is known, mucin plays a pivotal role in maintaining ocular surface homeostasis.[3] Therefore, two types of cell lines located on the ocular surface, namely HCECs and HCJECs, were employed here to evaluate the biocompatibility of PM hydrogels. Firstly, the cytocompatibility of PMPD copolymer was assessed using the CCK-8 assay. After co-culturing HCECs and HCJECs with different concentrations (0.1, 0.2, 0.5, 1, 2, 5, and 10 mg mL^{-1}) of PMPD for 24 and 48 h respectively, the cell viability of both HCECs (Fig. S9†) and HCJECs (Fig. S10†) remained over 80%, indicating favorable biocompatibility of zwitterionic PMPD copolymer which possesses cell membrane mimicking structure. In contrast, co-incubation with culture medium containing 10% DMSO (positive control) resulted in significantly reduced viability of both HCECs and HCJECs after 24 and 48 h (Fig. S11†), indicating the remarkable cytotoxicity of 10% DMSO. As for mucin and its derivatives-based biomaterials, numerous reports have substantiated their good biosafety.[12,66] Subsequently, hydrogel extracts were obtained by incubating

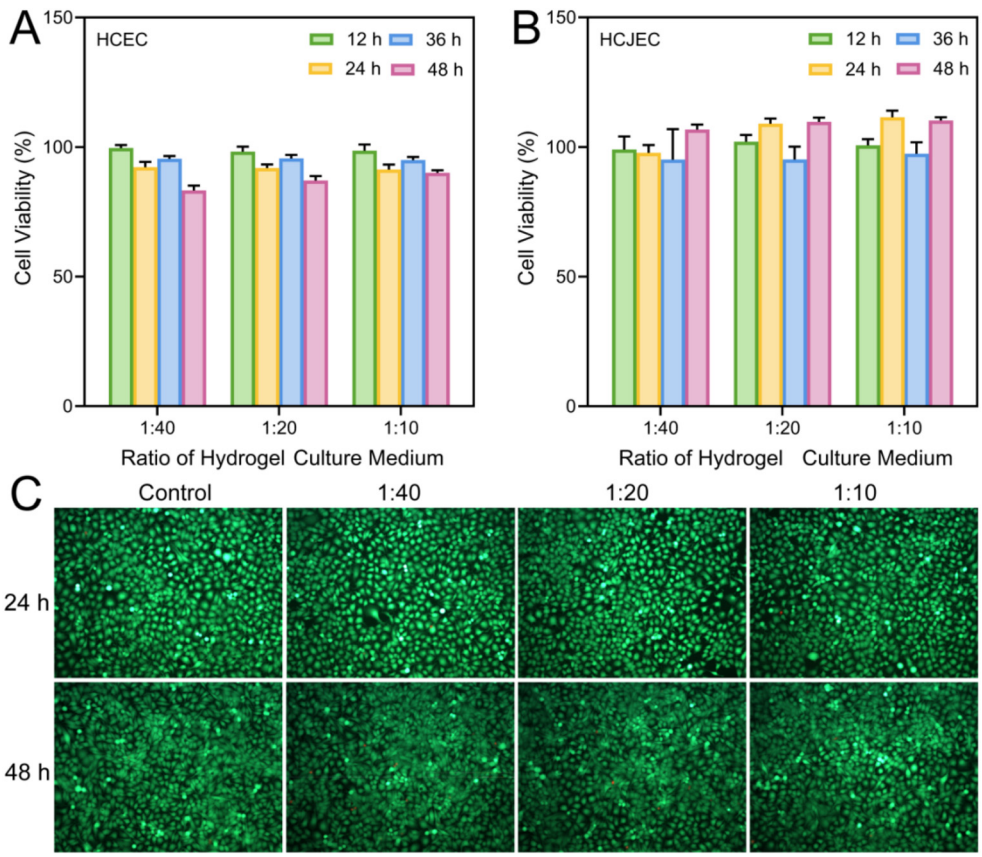

Fig. 6 *In vitro* biocompatibility of hydrogel extracts made from different hydrogel: culture medium volume ratios (1 : 40, 1 : 20, and 1 : 10). Cell viability of (A) HCECs and (B) HCJECs after co-incubation with hydrogel extracts for varying durations. (C) Images of Live/Dead staining assay of HCJECs after co-incubation with hydrogel extracts for 24 and 48 h.

PM hydrogels with culture medium at varying volume ratios (1 : 40, 1 : 20, 1 : 10). The cytocompatibility of PM hydrogel was further assessed through both CCK-8 assay and calcein-AM/ethidium homodimer-1 Live/Dead staining after co-culturing HCECs and HCJECs with hydrogel extracts. Both HCECs (Fig. 6A) and HCJECs (Fig. 6B) retained over 80% of cell viability after co-incubation with the hydrogel extracts for different durations up to 48 h, indicating minimal cytotoxicity towards these two types of cells. For Live/Dead staining, green fluorescent dye (calcein) was employed to label viable cells while red fluorescent dye (ethidium homodimer-1) was utilized to mark non-viable cells. Following a 24 h and a 48 h co-culture with hydrogel extracts, the majority of HCJECs were found to exhibit green fluorescence, with only a minimal fraction displaying red fluorescence (Fig. 6C), indicating negligible cytotoxicity. Additionally, there was a noticeable increase in cell density from 24 h to 48 h, implying that the hydrogel extracts exhibited no adverse effects on normal cellular growth and proliferation. Therefore, the above results validated the good biocompatibility of PM hydrogel, which is fabricated using naturally occurring mucin and nature-inspired MPC-based copolymer, highlighting its great potential for biomedical applications such as treating ocular surface diseases.

4. Conclusions

In summary, we successfully prepared mucus-inspired PM hydrogels through dynamic covalent chemistry. The hydrogels were formed by simply mixing solutions of zwitterionic PMPD copolymer and porcine gastric mucin, which was attributed to the formation of phenylboronic ester bonds between the PBA moieties of PMPD and diol residues of mucin. Due to the remarkable reversibility of phenylboronic ester bonds, the hydrogels exhibited favorable injectability, self-healing capability, and self-adaptability. Furthermore, both PMPD and mucin exhibited exceptional free radical scavenging ability, thereby conferring outstanding antioxidant activity upon the resulting PM hydrogels. The good biocompatibility of PM hydrogel was confirmed with both HCECs and HCJECs, benefiting from the cell membrane-biomimetic structure of MPC-based zwitterionic polymers as well as the natural origin of mucin. Our study broadens the scope of multifunctional mucin-based hydrogel preparation, showcasing their immense potential in mucosal drug delivery and the treatment of related diseases, particularly those associated with oxidative stress.

Author contributions

Chunwen Tao: methodology, data curation, formal analysis, investigation, writing – original draft preparation. Liyuan Peng: methodology, data curation, formal analysis, investigation, writing – original draft preparation. Qiuyun Shao: investigation, visualization. Kaihui Nan: resources, supervision, validation, funding acquisition. Ravin Narain: supervision, writing – review and editing. Yangjun Chen: conceptualization, supervision, funding acquisition, project administration, writing – review and editing. All authors have read and agreed to the published version of the manuscript.

Data availability

Detailed information about the design, synthesis and characterization are provided in the manuscript as well as the ESI.† Additional data will made available upon request from the corresponding authors.

Conflicts of interest

The authors declare no conflict of interest.

Acknowledgements

This work was financially supported by the National Natural Science Foundation of China (52003199), the Huadong Medicine Joint Funds of the Zhejiang Provincial Natural Science Foundation of China (LHDMY24H300003), the National Key R&D Program of China (2021YFA1101204), and the Zhejiang Provincial Natural Science Foundation of China (LQ20E030010).

References

1 C. Werlang, G. Cárcarmo-Oyarce and K. Ribbeck, *Nat. Rev. Mater.*, 2019, **4**, 134–145.
2 R. Bej, C. A. Stevens, C. Nie, K. Ludwig, G. D. Degen, Y. Kerkhoff, M. Pigaleva, J. M. Adler, N. A. Bustos, T. M. Page, J. Trimpert, S. Block, B. B. Kaufer, K. Ribbeck and R. Haag, *Adv. Mater.*, 2024, **36**, 2401745.
3 C. Baudouin, M. Rolando, J. M. Benitez Del Castillo, E. M. Messmer, F. C. Figueiredo, M. Irkec, G. Van Setten and M. Labetoulle, *Prog. Retin. Eye Res.*, 2019, **71**, 68–87.
4 C. Portal, V. Gouyer, F. Gottrand and J.-L. Desseyn, *Exp. Eye Res.*, 2019, **186**, 107724.
5 P. Argüeso, *Adv. Drug Delivery Rev.*, 2022, **180**, 114074.
6 M. Labetoulle, J. M. Benitez-Del-Castillo, S. Barabino, R. Herrero Vanrell, P. Daull, J. S. Garrigue and M. Rolando, *Int. J. Mol. Sci.*, 2022, **23**, 2434.
7 V. R. Kohout, C. L. Wardzala and J. R. Kramer, *Adv. Drug Delivery Rev.*, 2022, **191**, 114540.
8 G. Petrou and T. Crouzier, *Biomater. Sci.*, 2018, **6**, 2282–2297.
9 C. A. Rickert, B. Wittmann, R. Fromme and O. Lieleg, *ACS Appl. Mater. Interfaces*, 2020, **12**, 28024–28033.
10 B. Winkeljann, M. G. Bauer, M. Marczynski, T. Rauh, S. A. Sieber and O. Lieleg, *Adv. Mater. Interfaces*, 2020, **7**, 1902069.

11 C. A. Rickert, S. Mansi, D. Fan, P. Mela and O. Lieleg, *Macromol. Biosci.*, 2023, **23**, 2300198.
12 M. Marczynski, C. Kimna and O. Lieleg, *Adv. Drug Delivery Rev.*, 2021, **178**, 113845.
13 T. M. Lutz, C. Kimna and O. Lieleg, *Int. J. Biol. Macromol.*, 2022, **215**, 102–112.
14 R. Bej and R. Haag, *J. Am. Chem. Soc.*, 2022, **144**, 20137–20152.
15 K. Joyner, D. Song, R. F. Hawkins, R. D. Silcott and G. A. Duncan, *Soft Matter*, 2019, **15**, 9632–9639.
16 W. L. Brooks and B. S. Sumerlin, *Chem. Rev.*, 2016, **116**, 1375–1397.
17 L. Terriac, J.-J. Helesbeux, Y. Maugars, J. Guicheux, M. W. Tibbitt and V. Delplace, *Chem. Mater.*, 2024, **36**, 6674–6695.
18 M. Nakahata, N. Tominaga, K. Saito, K. Nishiyama, Y. Tanino, K. Saiki, M. Kojima and S. Sakai, *Macromol. Biosci.*, 2022, **22**, 2200055.
19 Y. Chen, W. Wang, D. Wu, H. Zeng, D. G. Hall and R. Narain, *ACS Appl. Mater. Interfaces*, 2019, **11**, 44742–44750.
20 P. Sun, T. Huang, X. Wang, G. Wang, Z. Liu, G. Chen and Q. Fan, *Biomacromolecules*, 2020, **21**, 556–565.
21 T. Figueiredo, J. Jing, I. Jeacomine, J. Olsson, T. Gerfaud, J. G. Boiteau, C. Rome, C. Harris and R. Auzely-Velty, *Biomacromolecules*, 2020, **21**, 230–239.
22 Y. Chen, D. Diaz-Dussan, D. Wu, W. Wang, Y.-Y. Peng, A. B. Asha, D. G. Hall, K. Ishihara and R. Narain, *ACS Macro Lett.*, 2018, **7**, 904–908.
23 M. Liu, J. Chen, L. Li, J. Zhou, R. Narain, K. Nan and Y. Chen, *J. Mol. Liq.*, 2024, **398**, 124239.
24 Y. Wu, Y. Wang, C. Zheng, C. Hu, L. Yang, Q. Kong, H. Zhang and Y. Wang, *Adv. Funct. Mater.*, 2023, **33**, 2305992.
25 Y.-Y. Peng, Q. Cheng, W. Wang, M. Wu, D. Diaz-Dussan, P. Kumar and R. Narain, *Polym. Chem.*, 2021, **12**, 5623–5630.
26 X. Deng, R. Attalla, L. P. Sadowski, M. Chen, M. J. Majcher, I. Urosev, D.-C. Yin, P. R. Selvaganapathy, C. D. M. Filipe and T. Hoare, *Biomacromolecules*, 2017, **19**, 62–70.
27 S. Pan, N. Zhang, X. He, Z. Fang, Y. Wu, Y. Wei and L. Tao, *ACS Macro Lett.*, 2023, **12**, 1037–1044.
28 Z. Shao, T. Yin, J. Jiang, Y. He, T. Xiang and S. Zhou, *Bioact. Mater.*, 2023, **20**, 561–573.
29 N. Mangiacotte, G. Prosperi-Porta, L. Liu, M. Dodd and H. Sheardown, *Nanomaterials*, 2020, **10**, 1400.
30 S. Liu, C. N. Chang, M. S. Verma, D. Hileeto, A. Muntz, U. Stahl, J. Woods, L. W. Jones and F. X. Gu, *Nano Res.*, 2014, **8**, 621–635.
31 X. Sun, Y. Sheng, K. Li, S. Sai, J. Feng, Y. Li, J. Zhang, J. Han and B. Tian, *Acta Biomater.*, 2022, **138**, 193–207.
32 H. Zou, Y. Hong, B. Xu, M. Wang, H. Xie and Q. Lin, *Acta Biomater.*, 2024, **185**, 441–455.
33 Q. Chen, X. Han, L. Liu, Y. Duan, Y. Chen, L. Shi, Q. Lin and L. Shen, *Biomacromolecules*, 2023, **24**, 5230–5244.
34 L. d'Amone, J. K. Sahoo, N. Ostrovsky-Snider, D. L. Kaplan and F. G. Omenetto, *Biomacromolecules*, 2023, **24**, 1310–1317.
35 N. Yoshinaga, J. K. Zhou, C. Xu, C. H. Quek, Y. Zhu, D. Tang, L. Y. Hung, S. A. Najjar, C. Y. A. Shiu, K. G. Margolis, Y.-H. Lao and K. W. Leong, *Nano Lett.*, 2023, **23**, 757–764.
36 C. L. G. Davidson, C. Deng, L. Trachsel, W. L. A. Brooks and B. S. Sumerlin, *Macromolecules*, 2024, **57**, 887–893.
37 Y. Chen, H. Han, H. Tong, T. Chen, H. Wang, J. Ji and Q. Jin, *ACS Appl. Mater. Interfaces*, 2016, **8**, 21185–21192.
38 B. Ren, R. Liu, Q. He, T. Wu, L. Song, H. Wang and J. Gu, *ACS Appl. Mater. Interfaces*, 2023, **15**, 9099–9109.
39 Q. Li, C. Wen, J. Yang, X. Zhou, Y. Zhu, J. Zheng, G. Cheng, J. Bai, T. Xu, J. Ji, S. Jiang, L. Zhang and P. Zhang, *Chem. Rev.*, 2022, **122**, 17073–17154.
40 A. B. Asha, Y. Chen and R. Narain, *Chem. Soc. Rev.*, 2021, **50**, 11668–11683.
41 Q. Jin, Y. Chen, Y. Wang and J. Ji, *Colloids Surf., B*, 2014, **124**, 80–86.
42 X. Yao, C. Qi, C. Sun, F. Huo and X. Jiang, *Nano Today*, 2023, **48**, 101738.
43 K. Ishihara, *Sci. Technol. Adv. Mater.*, 2022, **23**, 498–524.
44 W. Zhao, H. Wang, Y. Han, H. Wang, Y. Sun and H. Zhang, *ACS Appl. Mater. Interfaces*, 2020, **12**, 51236–51248.
45 X. Shi, D. Cantu-Crouch, V. Sharma, J. Pruitt, G. Yao, K. Fukazawa, J. Y. Wu and K. Ishihara, *Colloids Surf., B*, 2021, **199**, 111539.
46 K. Ishihara and K. Fukazawa, *J. Mater. Chem. B*, 2022, **10**, 3397–3419.
47 L. Ma, K. Li, J. Xia, C. Chen, Y. Liu, S. Lang, L. Yu and G. Liu, *J. Colloid Interface Sci.*, 2022, **610**, 923–933.
48 N. Iuster, O. Tairy, M. J. Driver, S. P. Armes and J. Klein, *Macromolecules*, 2017, **50**, 7361–7371.
49 R. Xie, H. Yao, A. S. Mao, Y. Zhu, D. Qi, Y. Jia, M. Gao, Y. Chen, L. Wang, D. A. Wang, K. Wang, S. Liu, L. Ren and C. Mao, *Nat. Biomed. Eng.*, 2021, **5**, 1189–1201.
50 G. Charmi, M. Rahimi, K. Socha, D. A. Pham, L. Séguy, Q. T. Phan, F. Moldovan, M. Kozanecki, K. Matyjaszewski, X. Banquy and J. Pietrasik, *Polym. Chem.*, 2023, **14**, 3827–3833.
51 J. Lu, X. Shen, H. Li and J. Du, *Exploration*, 2024, **4**, 20230142.
52 A. Bhattacharyya, R. Chattopadhyay, S. Mitra and S. E. Crowe, *Physiol. Rev.*, 2014, **94**, 329–354.
53 M. Dogru, T. Kojima, C. Simsek and K. Tsubota, *Invest. Ophthalmol. Visual Sci.*, 2018, **59**, DES163–DES168.
54 S. Li, Z. Lu, Y. Huang, Y. Wang, Q. Jin, X. Shentu, J. Ye, J. Ji, K. Yao and H. Han, *Adv. Sci.*, 2022, **9**, e2200435.
55 K. Li, Q. Gong, B. Lu, K. Huang, Y. Tong, T. E. Mutsvene, M. Lin, Z. Xu, F. Lu, X. Li and L. Hu, *Eye. Vis.*, 2023, **10**, 17.
56 H. Zou, H. Wang, B. Xu, L. Liang, L. Shen and Q. Lin, *Regener. Biomater.*, 2022, **9**, rbac070.
57 Z. Chen, Z. Li, N. Tang, Y. Huang, S. Li, W. Xu, Q. Wang, X. Chen, N. Zhao, Z. Zeng, Y. Xiao, X. Chen, J. Li, X. Zhou, G. Li, M. Yang and J. Huang, *Adv. Funct. Mater.*, 2024, **34**, 2307569.
58 G. Wei, W. Liu, Y. Zhang, Z. Zhou, Y. Wang, X. Wang, S. Zhu, T. Li and H. Wei, *Nano Lett.*, 2024, **24**, 2289–2298.
59 D. K. Min, Y. E. Kim, M. K. Kim, S. W. Choi, N. Park and J. Kim, *ACS Nano*, 2023, **17**, 24404–24416.

60 L. Yang, Y. Zeng, H. Wu, C. Zhou and L. Tao, *J. Mater. Chem. B*, 2020, **8**, 1383–1388.
61 X. Yang, J. Yang, Z. Ye, G. Zhang, W. Nie, H. Cheng, M. Peng, K. Zhang, J. Liu, Z. Zhang and J. Shi, *ACS Nano*, 2022, **16**, 4041–4058.
62 C. E. Cross, B. Halliwell and A. Allen, *Lancet*, 1984, **1**, 1328–1330.
63 S. Yuan, M. Hollinger, M. E. Lachowicz-Scroggins, S. C. Kerr, E. M. Dunican, B. M. Daniel, S. Ghosh, S. C. Erzurum, B. Willard, S. L. Hazen, X. Huang, S. D. Carrington, S. Oscarson and J. V. Fahy, *Sci. Transl. Med.*, 2015, **7**, 276ra227.
64 Y. Ogasawara, T. Namai, F. Yoshino, M.-C.-i. Lee and K. Ishii, *FEBS Lett.*, 2007, **581**, 2473–2477.
65 K. Jin, Y. Ge, Z. Ye, X. Pan, Y. Yan, Z. Mao and J. Ye, *Appl. Mater. Today*, 2022, **27**, 101411.
66 J. S. Brand, L. Forster, T. Böck, P. Stahlhut, J. Teßmar, J. Groll and K. Albrecht, *Macromol. Biosci.*, 2022, **22**, 2100274.